

# Shining a Light on Human Pose: On Shadows, Shading and the Estimation of Pose and Shape

Alexandru O. Bălan\*   Michael J. Black\*   Horst Haussecker†   Leonid Sigal\*

\*Department of Computer Science, Brown University, Providence, RI 02912, USA

†Intel Corporation, Santa Clara, CA 95054, USA

{alb, black, ls}@cs.brown.edu; horst.haussecker@intel.com

## Abstract

Strong lighting is common in natural scenes yet is often viewed as a nuisance for object pose estimation and tracking. In human shape and pose estimation, cast shadows can be confused with foreground structure while self shadowing and shading variation on the body cause the appearance of the person to change with pose. Rather than attempt to minimize the effects of lighting and shadows, we show that strong lighting in a scene actually makes pose and shape estimation more robust. Additionally, by recovering multiple body poses we are able to automatically estimate the lighting in the scene and the albedo of the body. Our approach makes use of a detailed 3D body model, the parameters of which are directly recovered from image data. We provide a thorough exploration of human pose estimation under strong lighting conditions and show: 1. the estimation of the light source from cast shadows; 2. the estimation of the light source and the albedo of the body from multiple body poses; 3. that a point light and cast shadows on the ground plane can be treated as an additional “shadow camera” that improves pose and shape recovery, particularly in monocular scenes. Additionally we introduce the notion of albedo constancy which employs lighting normalized image data for matching. Our experiments with multiple subjects show that rather than causing problems, strong lighting improves human pose and shape estimation.

## 1. Introduction

Strong illumination is often seen as a problem for pose estimation and tracking; this is particularly true for human pose estimation. In contrast, we show that, rather than hinder human pose and shape estimation, strong illumination can actually make it more robust. With a known light source, shadows and shading provide additional constraints for pose estimation and tracking. Conversely, if one has accurate pose estimates, we can estimate the light source lo-

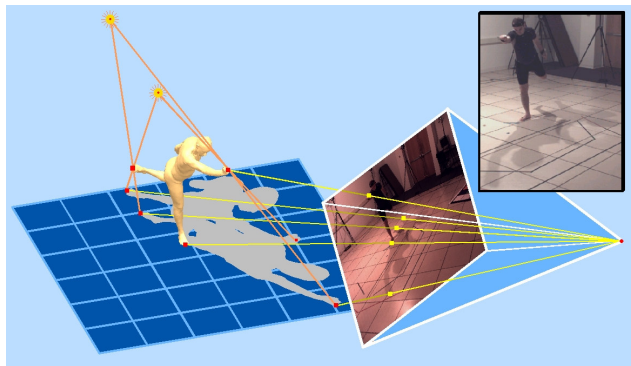


Figure 1. **The Shadow Camera.** Shadows cast on the ground may reveal structure not directly observed on an object such as the right arm or the left leg of the person in the image. The light together with the ground plane act like another camera view providing an additional silhouette of the object.

cation and reflectance properties of the body. Putting both of these observations together results in a complete framework for incorporating strong illumination in human pose estimation. These ideas, however, are applicable to object detection and tracking in general.

Consider the situation in which the scene is illuminated by a single, known, point light source and is viewed through one, or more, calibrated cameras. Here we focus on indoor scenes where the light source distance is finite. The approach, however, easily generalizes to distant light sources, the most common being the sun in outdoor scenes. Our first observation is that a point light source and the ground plane form what we call a *shadow camera*. The point light acts like the focal point of a pinhole camera with the ground plane acting like the image plane. The image formed on the ground is the shadow cast by the body (Figure 1). This can be generalized to multiple light sources (which effectively produce a “camera” with multiple focal points). The cast shadow image acts like a foreground silhouette mask in the image plane of a regular camera. Note, moreover, the “image plane” of the shadow camera need not be planar but can

be any calibrated surface (or surfaces) in the scene. This shadow image provides additional constraints on body pose which make it possible to estimate 3D pose from monocular camera views.

Making use of shadows requires the accurate segmentation of shadow regions in images. To that end we propose a novel approach that uses background subtraction data and checks whether putative shadow pixels are consistent with being on the calibrated ground plane. For a complete framework, we must also estimate the lighting in the scene automatically. We propose two approaches that exploit 3D body pose and shape represented using the SCAPE model [1], the parameters of which are estimated directly from image foreground silhouettes (without knowledge of scene illumination) [3].

The first approach recovers a point light position (or direction) from cast shadows. Using the known body pose in multiple frames and the detected shadow regions, we optimize for the light position that best explains the cast shadows. The second approach goes a step further and recovers both the light position, relative illumination strength, and albedo of the body. The key idea is the following: If we see the body in many different poses, then points on the body are seen at different orientations with respect to the unknown lighting. We assume that the albedo of the body does not change with pose and that any change in the appearance of a point on the body is due solely to its change in orientation with respect to the light. Combining many poses gives strong constraints on the location of the light, the albedo of the body and the background illumination in the scene. Hence by tracking an object with fixed lighting we can actually infer the lighting; in this way the human body becomes a *light probe* [4].

Finally we show that knowing the illumination allows us to remove the effects of lighting from images of the body. Given an estimated light position, light intensity, and background illumination, we solve for the albedo of points on the body in a given view. Then, rather than formulate the body tracking problem in terms of brightness constancy, we do so using *albedo constancy* and show that albedo constancy is less sensitive to changes in body pose.

We present results on multiple sequences with three light configurations and two subjects. A quantitative evaluation of pose estimation under different numbers of cameras and different numbers of point light sources is also provided.

## 1.1. Related Work

There is a long history of recovering lighting and using it to infer 3D structure. This work includes shape-from-shading, photometric stereo, shadow carving, inverse lighting, and reflectance modeling. A thorough survey is beyond the scope of this paper and the reader is referred to [7] for an overview.

Our work is quite different from the majority of work in shape, shading and lighting. Most approaches assume a fixed object which is viewed under different lighting conditions. The most common approaches attempt to estimate object shape from multiple images of a static object illuminated from different light locations (for example [5, 14]); in many cases these light locations are known. We turn this standard problem around and use multiple known poses (i.e. estimated from data) of the object to estimate the unknown lighting.

The most closely related work is that of [7] which estimates light sources and albedos using multiple views of an object. They assume a rigid object but move the camera to track it. This is similar to our case where the camera is static but the object moves. We go beyond their work to deal with an articulated non-rigid object which casts shadows on itself and the ground plane. They also only restrict attention to infinitely distant light sources and assume the depth variation of the object is small. In our case the light is a finite distance from the object (e.g. ceiling light) and the depth variation of the human body relative to the lighting distance is not negligible.

There are also many shape-from-shading and structured light methods that are related but beyond the scope of this paper (see [6, 15]). The most related method is that of Mercier *et al.* [8] which assumes unknown shape, reflectance and lighting. Like us they use silhouettes to reconstruct shape but unlike us use a voxel representation. They go beyond work here to recover more general reflectance models but have a much more limited capture environment and do not cope with the complexities of non-rigid and articulated objects. Our work could be extended to include their more general reflectance model. In related work Savarese *et al.* [10] use known light sources and estimate an unknown shape. In our case, we know the object shape in multiple frames and estimate the lighting.

There has been little work on articulated pose estimation from cast shadows. Segen and Kumar [11] describe a system to recognize basic hand gestures by tracking the 3D position and orientation of two fingers using the hand shadow captured with a single camera. More relevant is the work of Bruckstein *et al.* [2] in which they geometrically recover the pose of an articulated human stick figure and the light position from shadows. The approach requires the skeletal joints, and their corresponding locations on the shadow, to be manually marked in the image.

We apply a different strategy and define an objective function over the parametric pose and shape of the subject and the point light source position such that the projection of the shape onto the image silhouette and the shadow best overlap the observed body regions. We believe this to be the first automatic procedure to estimate articulated human pose and shape by taking advantage of cast shadows.

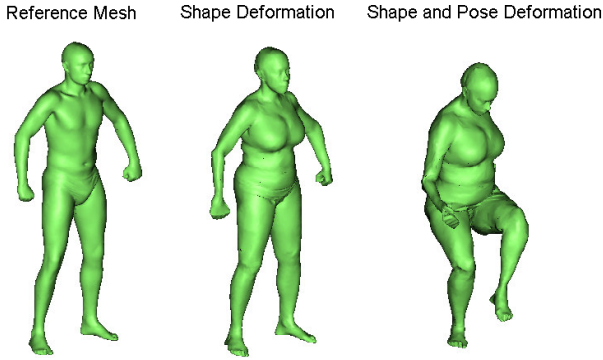


Figure 2. **Body Shape Model.** SCAPE [1] is a realistic triangulated mesh model that can represent different human body shapes and poses. The underlying low dimensional parameterization is given by  $(\tau, \theta, \beta)$ , specifying the global position  $\tau$ , limb rotations  $\theta$  and body eigen-shape coefficients  $\beta$  (here 6 DoF).

## 2. Pose & Shape from Silhouettes & Shadows

Much of the work on human pose estimation and tracking employs generative models of human shape that are crude approximations of the body. In recent work [3] we used a detailed graphics body model (SCAPE) [1], learned from range scans of real people, to address the problem of markerless human pose and shape estimation in a multi-camera setting (Figure 2). The generative model predicts silhouettes in each camera view given the pose/shape parameters of the the body and matches them to foreground silhouettes extracted from images using a fairly standard Chamfer distance measure. In this work we extend this framework to take advantage of shadows cast from point light sources. These shadows provide additional constraints on pose and shape which are sufficient to disambiguate and effectively enable monocular 3D pose estimation.

The new framework has the following steps: **1.** Segment the images into background, foreground and shadow regions (Section 2.1). **2.** Acquire initial estimates of the pose using a learned probabilistic mapping from image features to 3D pose (Section 2.2). **3.** Estimate pose and shape parameters from foreground silhouette data alone and generate the surface meshes in each frame (Section 2.3) [3]. **4.** Estimate light position from shadows (Section 2.4). **5.** Re-estimate pose and shape from foreground regions, shadow regions and the estimated light position (Section 2.3).

### 2.1. Foreground/Shadow Segmentation

Foreground silhouettes have been widely used in human pose estimation and tracking. Interestingly, most work in shadow detection has focused on *removing* the shadows to improve foreground segmentation [9]. Distinguishing foreground from shadows can be challenging since both differ significantly from the background. The initial step in

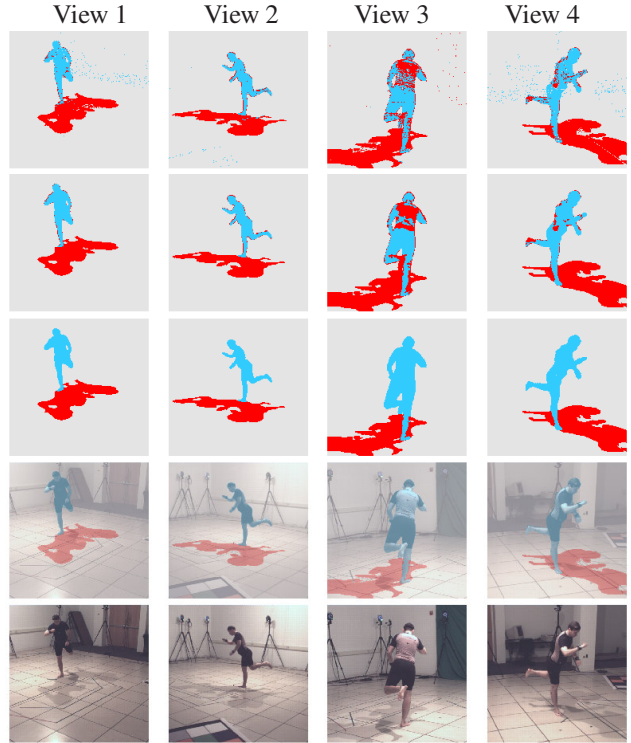


Figure 3. **Foreground and Shadow Segmentation.** Row 1: Per pixel classification. Row 2: Morphological operations. Row 3: Multi-view integration. Note the robustness introduced by this step. Row 4: Segmentation overlaid on original images. Row 5: Original images (with two light sources).

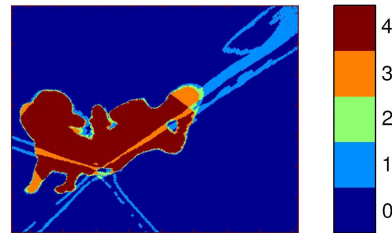


Figure 4. **Shadow Integration.** Segmented shadow regions from Figure 3 aligned in a single coordinate frame. Each registered shadow can be thought of as voting for the presence of a shadow. Regions that contain only one vote (light blue) can be classified as outliers and potentially relabeled as foreground pixels.

shadow detection is fairly standard and involves first transforming the images into HSV color space (Hue, Saturation, Value), then classifying foreground, shadow, and background classes using only the saturation channel. This is followed by several morphological operations, including median filtering, image dilation and erosion, removal of small disconnected components and hole filling. Rows 1 and 2 in Figure 3 show the segmentation result before and after this procedure.

We employ a novel shadow segmentation method that uses multiple synchronized and calibrated camera views

of the scene and a calibrated ground plane on which the shadow is cast. It is based on the observation that each shadow pixel corresponds to a 3D ray which can be intersected with the ground plane with known coordinates. Therefore each camera view yields a 3D reconstruction of the shadow.

Ideally, the 3D image of the shadow is the same in all views. In practice, the segmented shadow regions differ due to noise in the segmentation and the fact that the body may occlude the shadow from some camera views. We think of the recovered shadow in each view as voting for the true 3D shadow as illustrated in Figure 4. Inconsistent 3D shadow reconstructions result, in part, from mislabeling foreground as shadow. For example, in Figure 3, View 3, most of the torso is detected as shadow, yet it is not consistent with the shadow reconstructions in the other views.

We adopt a conservative approach and attempt to relabel inconsistent shadow regions only when it leads to a spatially consistent foreground segmentation. More precisely, we relabel shadow pixels as foreground when they are not explained by the other shadow views *and* are adjacent to foreground pixels in the current view. This step may alter the shadow vote outcome. Consequently, the procedure is repeated until convergence (typically 3 to 5 iterations), resulting in robust and clean segmentations (see Figure 3).

## 2.2. Initialization of Pose

Our optimization strategy requires an initial estimate of the pose that is relatively close to the true configuration. In [3] we relied on a cylindrical body model to perform human tracking and initialize the SCAPE optimization. This was shown to work well in a multi-camera setup, but still required initialization at the first frame. Here we adopt a fully automatic strategy that is able to cope with pose ambiguities in monocular sequences. We use a Bayesian Mixture of Experts (BME) framework [13] to learn a direct non-linear probabilistic mapping from image features to the 3D pose. The image (shape context) features are computed from foreground silhouettes in one or more views. While we can sample multiple initial poses from this model, we choose only the most likely here and assume the body shape is the mean shape in the SCAPE model.

## 2.3. Optimization

Our goal is to estimate the shape and pose of the body along with the light position(s) from one or more images; we do so within a framework of *synthesis and evaluation*. Given a predicted body shape and pose described by the state vector  $s = (\tau, \theta, \beta)$  (see Figure 1), we project the 3D surface mesh into the image plane of camera  $i$  to produce an estimated foreground  $F_i^e(s)$ . This is then compared with the observed foreground  $F_i^o$ . Given a light position  $\mathbf{c}$ , ground plane  $\mathbf{g}$ , and a canonical view  $i$ , the estimated

shadow,  $S^e(s, \mathbf{c}, \mathbf{g})$ , of the surface mesh on the ground is rendered in view  $i$  and compared with the observed shadow  $S^o$  (where  $S^o$  is the shadow derived from multiple views and transformed into the canonical view (e.g. Fig. 4)).

To estimate the model and light parameters, we formulate an objective function in terms of a *silhouette dissimilarity measure*,  $D(\cdot^e, \cdot^o)$ , which is implemented as a bi-directional Chamfer distance between estimated and observed silhouettes [3]. In [3] we rely on foreground silhouettes alone to estimate pose and shape; here we add a term to measure the shadow difference. To optimize pose and shape from silhouettes and shadows we minimize

$$E(s) = D(S^e(s, \mathbf{c}, \mathbf{g}), S^o) + \sum_{i=1}^K D(F_i^e(s), F_i^o) \quad (1)$$

where  $K$  one or four camera views in our experiments. In all cases, the optimization is performed using a stochastic search technique related to annealed particle filtering as described in [3].

## 2.4. Estimating the Light Position

To estimate light position, we first compute the pose and shape,  $s_t$ , for some number of time instants  $t = 1 \dots N$  in a sequence. Keeping pose and shape fixed, we then optimize for the light position  $\mathbf{c}$  by minimizing the silhouette distance

$$E(\mathbf{c}) = \sum_t D(S^e(s_t, \mathbf{c}, \mathbf{g}), S_t^o) \quad (2)$$

where the difference is computed between the shadow predicted by the model,  $S^e(s_t, \mathbf{c}, \mathbf{g})$ , and the one computed from the image(s) at time  $t$ ,  $S_t^o$ .

To initialize the search we parameterize the light location by its height from the floor and its azimuth and elevation angles. We discretize the space in a reasonable range above the person and compute the value of (2) for a total of 288 light positions. We then select the best location, re-discretize around it using a  $7 \times 7 \times 7$  grid with a finer sampling, and repeat down to a  $5mm$  discretization.

## 2.5. Results

The experiments here use three sequences, ( $R^1$ ,  $R^2$  and  $R^{1,2}$ ), the first two with different individual light sources, and the third having both lights turned on. Each sequence was captured by four synchronized and calibrated color cameras. Sequences  $R^1$  and  $R^{1,2}$  are of subject AB while  $R^2$  contains subject MB. In all cases we fit the parameters of a SCAPE body model, independently in each frame, as described in [3]. Ground truth light positions were computed using a commercial motion capture system.

**Light estimation results:** We first show how the light position can be estimated from the body model and extracted shadows. In each sequence the shape and pose of

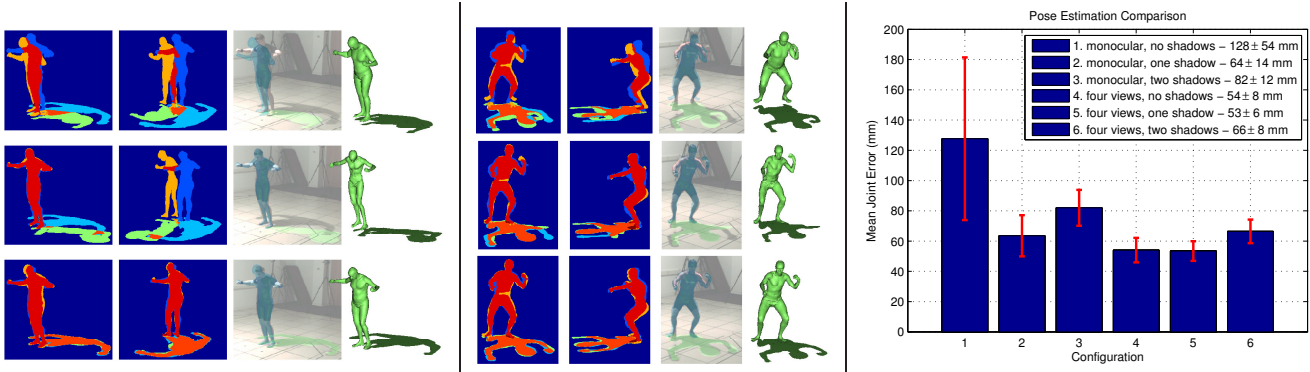


Figure 5. **Effect of shadows on pose and shape estimation.** *Left* ( $R^1$ , AB) and *Middle* ( $R^2$ , MB): **Monocular** shape and pose estimation. Row 1 shows the automatic initialization (Section 2.2). Row 2 shows estimated pose and shape based on monocular silhouette optimization. Row 3 shows the improvement obtained by adding shadows to the optimization. Color key: amber =  $F^e$ ; mid-blue =  $F^o$ ; red = agreement between  $F^o$  and  $F^e$ ; light green =  $S^e$ ; light blue =  $S^o$ ; orange = agreement between  $S^o$  and  $S^e$ . The estimation uses only the left-most view of each frame, with the other view presented for visual inspection. The right two images in the panes show the recovered 3D shape projected into the image and rendered in green along with its shadow. *Right*: Quantitative evaluation of the pose reconstruction using different numbers of lights and camera views for optimization. Shadows prove most useful for monocular sequences when generated by a single point light source. (See <http://www.cs.brown.edu/research/vision/scape> for videos and additional results.)

	Placement Error	Relative Distance Error	Direction Error
Light 1	140mm	4.64%	$0.87^\circ$
Light 2	218mm	7.40%	$1.83^\circ$

Table 1. Estimated light position and distance accuracy. Light 1 was estimated with subject AB (sequence  $R^1$ , 10 poses) and Light 2 with subject MB (sequence  $R^2$ , 10 poses).

the subject was estimated at several time instants using only the foreground silhouettes as image observations. Given the estimated shape and pose, we optimize (2) as described in Section 2.4. Each pose results in a different shadow and provides different constraints on the light position. We evaluate the estimated light positions in terms of both direction and position error. In particular, we report the relative distance error as a ratio of the placement error and the distance from the light source to the average location of the subject on the floor (Table 1).

The results suggest that the cast shadows were very good for recovering the light direction, but not the precise location. This is due to the fact that small changes in the direction of incoming light induce large changes in the cast shadow while, at the distances found here, variation in distance produces smaller changes.

**Pose and shape fit:** Here we use the estimated light positions from above along with the cast shadows to constrain the estimation of the SCAPE parameters (1). We evaluate how effectively a shadow camera can replace a video camera (in some applications an additional light source may be more practical than an additional camera).

First, consider the *monocular* pose and shape estimation problem. Figure 5 shows examples of the initialization (top

row), estimated pose and shape based on monocular foreground silhouettes alone (middle row), and using both foreground and shadows (bottom). The example to the left illustrates why monocular views are inherently ambiguous and the optimization is under-constrained. While the fit of the foreground in the optimized view is almost perfect, an alternate camera view reveals that the recovered pose is far from the truth; note also that the projected shadow (light green) does not match the observed shadow (light blue). The shadow in this case is sufficient to fully constrain the pose and shape estimation (bottom). This demonstrates that shadows can provide powerful constraints for human pose and shape estimation from monocular images.

We quantitatively evaluate pose recovery accuracy using joint placement error. Our video capture was synchronized with a marker-based motion capture system which was used to acquire ground truth joint locations for each frame. We compute the root mean squared joint location error in *mm* for the hips, knees, ankles, shoulders, elbows and wrists. Figure 5 (right) shows the mean and standard deviation of the errors over all the joints. The results suggest that a single shadow offers a significant improvement in monocular pose estimation. The addition of a second point light source actually reduced accuracy, but additional experiments are needed before we can make any conclusive statements about the effects of multiple light sources on pose accuracy. Once four camera views are available, shadows appear to offer no clear benefit.

The spatial configuration of the camera, light source and the subject affect the performance of the system. Intuitively, a cast shadow is most informative when the camera viewing direction is orthogonal to the plane containing the light

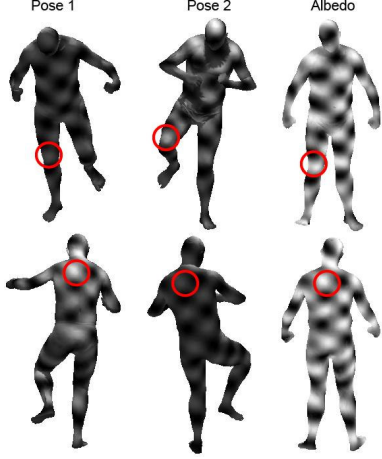


Figure 6. **Illumination from pose; synthetic example.** Multiple body poses are shown for a fixed lighting configuration. Corresponding points on the body have the same albedo but appear different due to changes in their orientation with respect to the light source. *Right:* estimated albedo.

and subject. If the light, camera and subject are relatively collinear, then there is little new information present in the shadow. We conclude that cast shadows may provide an inexpensive means to generate a “second view” for pose estimation in a controlled environment with a single camera.

### 3. Lighting from Shading and Pose

In addition to cast shadows on surfaces in the world, the human body itself contains information about the lighting in the scene. In particular, shading on the limbs and shadows cast by one body part onto another are a rich source of lighting and shape information. Exploiting this requires accurate knowledge of the body shape (and consequently the surface normals) which is provided by the SCAPE model. We assume that the body albedo does not change with pose (a reasonable assumption), the illumination is from a single point light source (this can be generalized as discussed below), the light source is not moving (reasonable in most scenes), and that the reflectance is Lambertian (violated in practice but sufficient for our purposes). Each body pose provides corresponding surface points in different orientations relative to the light which provide constraints on the albedo, light position and light intensity. By combining constraints from multiple poses we infer the illumination in the scene and albedo of the body.

This is illustrated in Figure 6. Using known poses/shapes we generated synthetic views of the scene with a known albedo (sinusoidal plaid pattern) and known illumination. Using the method below we automatically inferred the light position, the albedo and the illumination strength (up to a scale factor). The recovered albedo shown on the right looks “flat” with all the shading information removed.

### 3.1. Reflectance Model

Let  $\mathbf{a} = [a_1 \dots a_V]^T$  be a vector containing the albedo at each of  $V$  vertices in the body mesh and let  $N_p = [\mathbf{n}_{1,p} \dots \mathbf{n}_{V,p}]^T$  be a matrix of surface normals at each vertex for the  $p^{th}$  body pose. We saw above that body shape and pose can be estimated reliably from silhouettes; this gives us  $P$  body poses with known 3D coordinates  $X_p = [\mathbf{x}_{1,p} \dots \mathbf{x}_{V,p}]$  at each vertex. Here each pose is seen in four camera views and the visibility of each point from each camera is easily computed.

If  $\mathbf{c}$  is the location of a single point light source, then  $\mathbf{s}_{v,p}(\mathbf{c}) = \mathbf{c} - \mathbf{x}_{v,p}$  defines a light direction from the vertex  $v$  in pose  $p$  to the light source. Finally let  $d_{v,p}$  be the distance from the light to the body vertex in pose  $p$ . We represent the appearance of the body,  $\hat{r}_p$ , in a given pose using the standard Lambertian reflectance model. For vertexes that are in direct illumination the reflectance is

$$\hat{r}_{v,p} = a_v ((\mathbf{s}_{v,p}(\mathbf{c}))^T \mathbf{n}_{v,p} l / (d_{v,p}(\mathbf{c}))^2 + b) \quad (3)$$

where  $l$  is the light intensity and  $b$  is the background illumination. For body points in shadow we have  $\hat{r}_{v,p} = a_v b$ .

Given observed images we compute the error

$$E(l, b, \mathbf{a}, \mathbf{c}) = \frac{1}{Z} \sum_{p=1}^P \sum_{k=1}^K \sum_{v=1}^V \text{vis}(p, k, v) \rho(r_{p,k,v} - \hat{r}_{p,k,v})$$

where  $\text{vis}(p, k, v) = 1$  if vertex  $v$  is visible from camera  $k$  in pose  $p$  and zero otherwise; the same indexing notation is used for the observed and estimated reflectance  $r_{p,k,v}$  and  $\hat{r}_{p,k,v}$ . The normalization term  $Z$  is simply the sum of the visible pixels. Here we formulate the error using a robust function  $\rho()$  to account for: 1) inaccuracies in pose and shape estimation which may produce erroneous surface normals; 2) limitations in the body model (e.g. the body model is naked while actual subjects wear clothes); 3) violations of the Lambertian assumptions (e.g. skin typically has a specular component). Here we take  $\rho()$  to be the negative log Student-t function.

Note that there is a well known ambiguity in that one can multiply the albedo by a constant factor and scale  $l$  and  $b$  appropriately to compensate. Consequently we set  $l$  to be an arbitrary constant and find  $\mathbf{a}$  and  $b$  relative to that. Note also that it is trivial to change the formulation to model a light source at infinity and estimate light source direction rather than position (in this case all rays  $\mathbf{s}$  are parallel and the light intensity does not vary with distance).

Finally, most previous models have looked at objects with limited depth variation relative to the distance from the light source and, hence, have ignored the  $1/d^2$  term. We argue for people tracking in indoor environments this term cannot be safely ignored as we observe significant intensity variation from a person’s head to their feet with illumination mounted on the ceiling. If there is sufficient variation in

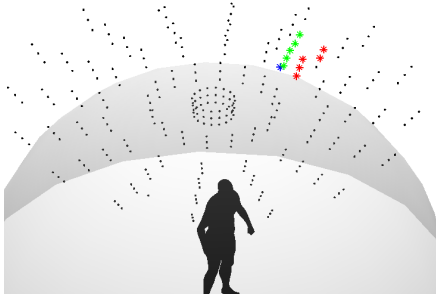


Figure 7. **Estimated light position; synthetic example.** Black dots represent the course initializations of the light. Red stars are the initial locations with lowest error. Green are the the result of optimization starting with the red stars. Blue is the ground truth.

depth of points across poses, this quadratic fall-off of light intensity helps constrain the distance of the light source.

### 3.2. Optimization

Minimizing  $E(l, b, \mathbf{a}, \mathbf{c})$  takes place in two stages. First a coarse initialization search is performed. Assuming a single point light source we discretize the space as in Section 2.4 (see Figure 7). Given each hypothesized light position we solve for  $\mathbf{a}$  and  $b$  (recall  $l$  is fixed) using coordinate descent. The background illumination is initialized to  $b = 0$  and the albedo to a constant value over the entire body. The five light positions with the lowest residual error are selected as initial starting locations.

The algorithm then optimizes over the all the parameters including the light source location,  $\mathbf{c}$ , using coordinate descent; note we enforce positivity constraints on the albedo and background illumination during optimization. Convergence is determined when the change in the residual  $E(l, b, \mathbf{a}, \mathbf{c})$  is less than a threshold for five iterations. The gradients with respect to the parameters are all straightforward except for those related to light position. Changes in light position change which vertexes are directly illuminated; computing the gradient with respect to these changes cannot be done in closed form and approximating it is too computationally costly since it involves multiple visibility computations. Consequently, we approximate the gradient with respect to  $\mathbf{c}$  by simply ignoring these changes in illuminated vertexes. Still, at each iteration of the descent, the visibility with respect to the light must be computed and this is the most computationally expensive part of the algorithm. Current visibility computations are performed in Matlab and take about one second per view; this could be reduced with graphics hardware.

### 3.3. Albedo and Lighting Results

We evaluate the method using a synthetic sequence ( $S^1$ ) where all parameters are known and two real sequences ( $R^1$ , 83 poses and  $R^2$ , 23 poses).  $S^1$  was constructed using



Figure 8. **Estimated albedos** for two different subjects and light positions.

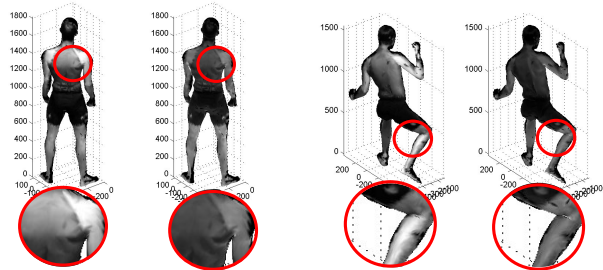


Figure 9. **Albedo constancy.** Given known lighting, we undo its effect in images. Several views of the body are shown viewed from different cameras in different poses. In each pair, the left shows the visible pixel luminance values while the right shows these values “corrected” to remove lighting. Note that the effects of illumination are greatly reduced.

the same body shapes and lighting as  $R^1$  but the observations were generated using the model (3) and a synthetic albedo. To recover the albedo in the real sequences, we first converted the input images to a single luminance channel (sum of RGB values) and excluded pixels that were saturated (pixels values in the top 10% for a given frame).

Figure 7 shows the recovered light position for  $S^1$ . Despite having a unique minimum, we found the distance of the light source was weakly constrained in practice (lying along a line). The position was fairly accurately recovered with the best estimate being  $56.3mm$  (1.86%) from the truth. The estimated albedo accounted for for 98% of the variance in the true albedo.

For the real sequences the camera positions were consistently biased below the true position. The error in position was  $506.2mm$  (16.7%) for  $R^1$  and  $412.7mm$  (12.67%) for  $R^2$ . Here we posit that a non-linear camera response near saturated regions caused the bias. The recovered albedos for the two sequences are shown in Figure 8. In both cases, the estimated albedo appropriately lacks most of the shading information present in the input data.

### 3.4. Albedo Constancy

Changes in orientation with respect to the light source cause changes in luminance; these violate the common assumption of brightness constancy used in many tracking frameworks. In human tracking, these illumination effects can be significant [12]. Given estimated light position (or direction), light intensity, and background illumina-

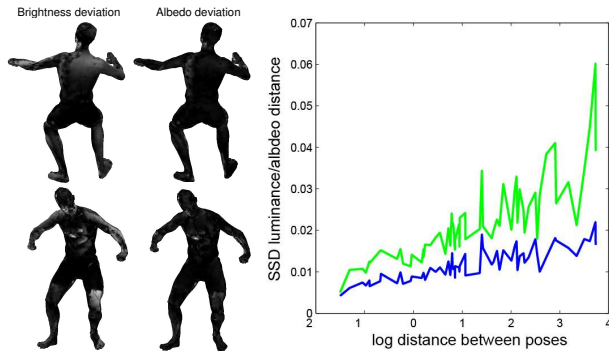


Figure 10. **Brightness versus albedo constancy.** *Left:* standard deviation computed for brightness (left) and albedo (right) for every point on the body. *Right:* Sum of squared differences in corresponding mesh locations plotted as a function of the log distance between poses defined in terms of surface normals. Green: brightness constancy error; Blue: albedo constancy error.

tion, along with the body surface normals, we solve for the albedo of the body in each frame using (3). We can then define tracking in terms of *albedo constancy* rather than brightness constancy.

While tracking is not the focus of this paper, we show preliminary evidence that albedo constancy may be more reliable than brightness constancy. For subject MB, we used the estimated illumination to compute the albedo in each frame and normalized both the albedo values and brightness values to  $[0, 1]$ . Figure 9 shows two poses from  $R^2$  with the original brightness on the left and the albedo on the right after removing lighting effects. Figure 10 shows the standard deviation in the pixel values for both brightness and albedo. Observe that the legs, arms, and back all have high deviation in the brightness model since their orientation changes significantly throughout the sequence. Figure 10 (right) shows the squared errors (SSD) between corresponding points on the body in different poses as a function of the log distance between poses (defined in terms of the dot product between corresponding surface normals). As expected, albedo is less sensitive to changes in surface pose.

## 4. Conclusions

We have presented a framework for exploiting strong lighting in the estimation of 3D human shape and pose. We have shown that a sufficiently rich model of the human body makes estimation of light sources practical. We have also shown that knowing the lighting in a scene can make human pose estimation more reliable. In contrast to the prevailing wisdom that strong lighting should be avoided, or that vision algorithms should be invariant to lighting, we show that strong lighting is actually beneficial to pose and shape estimation. These conclusions extend beyond the case of human pose considered here.

In future work we will explore the use of albedo con-

stancy for tracking. Future work will also consider extended light sources (which can be modeled as many point light sources) and will combine cast shadows with shading for light source estimation. We will also explore more complex reflectance models. Finally we will explore the integration of shading information into the body shape fitting.

**Acknowledgments.** This work was supported by NSF grants IIS-0534858 and IIS-0535075 and a gift from Intel Corp. We thank James Davis for useful discussions. Portions of this work were performed by MJB and AOB at Intel; MJB is a consultant for Intel Corp.

## References

- [1] D. Anguelov, P. Srinivasan, D. Koller, S. Thrun, J. Rodgers, and J. Davis. SCAPE: Shape completion and animation of people. *SIGGRAPH*, 24(3):408–416, 2005.
- [2] A. M. Bruckstein, R. J. Holt, Y. D. Jean, and A. N. Netravali. On the use of shadows in stance recovery. *Int. J. Imaging Systems and Tech.*, 11(5):315–330, 2001.
- [3] A. O. Bălan, L. Sigal, M. J. Black, J. E. Davis, and H. W. Haussecker. Detailed human shape and pose from images. In *CVPR*, 2007.
- [4] P. Debevec. Rendering synthetic objects into real scenes: Bridging traditional and image-based graphics with global illumination and high dynamic range photography. In *SIGGRAPH*, pages 189–198, 1998.
- [5] R. Epstein, A. Yuille, and P. Belhumeur. Learning object representations from lighting variations. In *Int. W. Object Rep. in Comp. Vis. II*, pages 179–199, 1996.
- [6] C. Lin and R. Nevatia. Building detection and description from a single intensity image. *CVIU*, 72(2):101–121, 1998.
- [7] Q.-T. Luong, P. Fua, and Y. Leclerc. The radiometry of multiple images. *PAMI*, 24(1):19–33, 2002.
- [8] B. Mercier, M. D. and A. Fournier. A framework for automatically recovering object shape, reflectance and light sources from calibrated images. *IJCV*, 73(1):77–93, 2007.
- [9] A. Prati, I. Mikic, M. M. Trivedi, and R. Cucchiara. Detecting moving shadows: Algorithms and evaluation. *PAMI*, 25(7):918–923, 2003.
- [10] S. Savarese, M. Andreetto, H. Rushmeier, F. Bernardini, and P. Perona. 3D rconstruction by shadow carving: Theory and practical evaluation. *IJCV*, 71(3):305–336, 2007.
- [11] J. Segen and S. Kumar. Shadow gestures: 3D hand pose estimation using a single camera. *CVPR*, 1:479–485, 1999.
- [12] H. Sidenbladh and M. Black. Learning the statistics of people in images and video. *IJCV*, 54(1–3):182–209, 2003.
- [13] C. Sminchisescu, A. Kanaujia, Z. Li, and D. Metaxas. Discriminative density propagation for 3D human motion estimation. *CVPR*, I:390–397, 2005.
- [14] A. L. Yuille, D. Snow, R. Epstein, and P. N. Belhumeur. Determining generative models of objects under varying illumination: Shape and albedo from multiple images using svd and integrability. *IJCV*, 35(3):203–222, 1999.
- [15] R. Zhang, P.-S. Tsai, J. Cryer, and M. Shah. Shape from shading: A survey. *PAMI*, 21(8):690–706, 1999.